Mean-field fluid behavior of the Gaussian core model

A. A. Louis, P. G. Bolhuis, and J. P. Hansen
Department of Chemistry, Lensfield Road, Cambridge CB2 1EW, United Kingdom
(Received 4 July 2000)

We show that the Gaussian core model of particles interacting via a penetrable repulsive Gaussian potential, first considered by Stillinger [J. Chem. Phys. **65**, 3968 (1976)], behaves as a weakly correlated ''mean-field fluid'' over a surprisingly wide density and temperature range. In the bulk, the structure of the fluid phase is accurately described by the random phase approximation for the direct correlation function, and by the more sophisticated hypernetted chain integral equation. The resulting pressure deviates very little from a simple mean-field-like quadratic form in the density, while the low density virial expansion turns out to have an extremely small radius of convergence. Density profiles near a hard wall are also very accurately described by the corresponding mean-field free-energy functional. The binary version of the model exhibits a spinodal instability against demixing at high densities. Possible implications for semidilute polymer solutions are discussed.

PACS number(s): 61.20.Gy, 61.25.Hq, 83.70.Hq

I. INTRODUCTION

Interactions between atoms or molecules in simple fluids invariably contain a short-range repulsive component or hard core, such that the local molecular structure is dominated by excluded volume effects. This observation explains the success of simple models involving hard convex bodies in explaining the structure and phase transitions in simple atomic or molecular fluids [1]. For example, the hard sphere model has been instrumental in understanding freezing of simple fluids [2]. The same success extends to somewhat more complex fluids such as liquid crystals, where hard ellipsoids or spherocylinders have been widely used to investigate the isotropic-to-nematic transition and other mesophases [3]. However, the situation is generally not as simple in complex fluids, where effective interactions between mesoscopic particles are often of entropic origin. While excluded volume effects still dominate the interaction between compact colloidal particles, the effective forces between ''soft'' or fractal objects of fluctuating shape, such as polymer coils or membranes, cannot be modeled by hard cores. Polymers in a good solvent form highly penetrable coils and it is by now well established that the effective interaction between the centers of mass of two polymer coils, duly averaged over internal conformations, is finite for all distances, and decays rapidly beyond the radius of gyration of the coils [4–7]. For two isolated nonintersecting polymer chains, the effective pair potential at zero separation of the centers of mass, $v(r=0)$, is of the order of $2k_BT$ for sufficiently long chains [6,7], and is reasonably well represented by a Gaussian whose width is of order the polymer radius of gyration R_G, as shown in Fig. 1.

We have recently shown that the general shape of the effective pair potential remains roughly the same in dilute and semidilute solutions of self-avoiding random walk (SAW) polymers, and does not vary strongly with polymer concentration (see Fig. 1) [8]. The effective pair potential model has been shown to accurately reproduce the structure and thermodynamics calculated from Monte Carlo (MC) simulations of solutions of SAW polymers over a wide range of concentrations [8].

Neglecting in the first instance the state dependence of the effective potential, it seems hence worthwhile to examine the equilibrium properties of a fluid of ''soft'' particles interacting via a pair potential approximated by a simple Gaussian form

$$v(r)=\epsilon\exp\left(-\frac{r^2}{R^2}\right), \tag{1}$$

where ϵ is the energy scale and R determines the width. The Fourier transform (FT) is

$$\hat{v}(k)=\pi^{3/2}R^3\epsilon\exp\left(-\frac{k^2R^2}{4}\right). \tag{2}$$

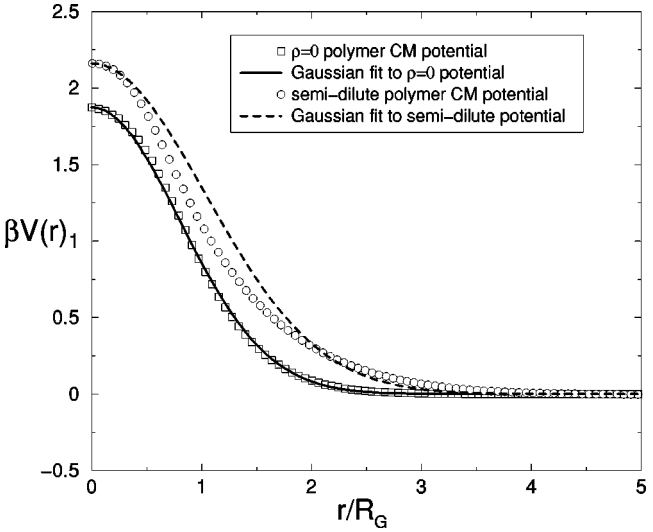

FIG. 1. Polymer center of mass potentials $\beta v(r)$ from simulations of $L=500$ monomer SAW chains [8] are compared to a best-fit Gaussian (1), determined by fitting $\beta v(0)$ to fix $\beta\epsilon$, and $\beta\hat{v}(0)$ to fix R. The potential for two isolated coils ($\rho\to 0$) is well approximated by a Gaussian potential with $\beta\epsilon=1.87$, $R=1.13R_G$. The potential in the semidilute regime [$\rho\sim 4\times 3/(4\pi R_g^3)$] is approximated by a Gaussian potential with $\beta\epsilon=2.16$, $R=1.45R_G$.

Such a ''Gaussian core model'' (GCM) was in fact introduced some time ago by Stillinger [9], who focussed on the low-temperature regime $\epsilon^* = \epsilon/k_B T \gg 1$, where the model exhibits hard-sphere-like behavior, and a reentrant fluid-solid-fluid phase diagram under compression below a threshold temperature. This work was further expanded by Lang *et al.* [10], who showed that the model remains fluid at all densities when $\epsilon^* \lesssim 100$. They also demonstrated that for this model, the familiar hypernetted chain (HNC) closure for the pair distribution function $g(r)$ becomes exact in the high density limit, and that the random phase approximation (RPA) is remarkably accurate at high densities.

In this paper we concentrate on the fluid phase of the GCM ($\epsilon^* < 100$), with a particular emphasis on the regime relevant for polymer solutions ($\epsilon^* \simeq 2$) [8], for which the dilute regime corresponds to reduced densities $\rho^* = \rho R^3 \lesssim 3/(4\pi) \approx 0.239$, and the semidilute regime corresponds to $\rho^* \gtrsim 3/(4\pi)$ [11] (here $\rho = N/V$ is the number of Gaussian core particles per unit volume). We shall successively consider the homogeneous fluid phase, the inhomogeneous fluid phase in the vicinity of a hard wall, and the possibility of demixing of binary Gaussian core systems.

II. THE HOMOGENEOUS FLUID PHASE

A. The thermodynamic stability of the GCM fluid

We consider a system of N particles interacting via a Gaussian pair potential (1), in a volume V. In the absence of an infinitely repulsive core, the first question is that of thermodynamic stability against collapse, i.e., the existence of a well defined thermodynamic limit. According to definition 3.2.1. in Ruelle's classic book [12], the total interaction energy V_N, which can be built up of pair and higher order potentials, is *stable* if there exists a $B \geqslant 0$ such that

$$V_N(\mathbf{r_1}, \ldots, \mathbf{r_N}) \geqslant -NB \tag{3}$$

for all $N > 0$ and all $\{\mathbf{r_i}\}$ in the phase space R^N. Stability implies convergence of the grand partition function and a well defined thermodynamic limit. Specializing to pair potentials v_2, the total potential energy of the system, for any configuration of N particles $\{\mathbf{r_i}\} \in R^N$, can be written as

$$V_N^{(2)}(\mathbf{r_1}, \ldots, \mathbf{r_N}) = \sum_{1 \leqslant i < j \leqslant N} v_2(|\mathbf{r_i} - \mathbf{r_j}|). \tag{4}$$

For purely repulsive pair potentials, such as the GCM with $\epsilon^* \geqslant 0$, $V_N^{(2)}$ satisfies the condition (3), so that a well defined thermodynamic limit exists. However, if $v_2(r)$ is not strictly positive, this may no longer be true. In Appendix A two examples are discussed, involving a finite core and (small) attractive tail, which do not lead to a proper thermodynamic limit.

B. The structure of the GCM fluid

To determine the pair structure of the GCM fluid, we have used the HNC closure which becomes exact in the high density limit; this closure relates the direct correlation function $c(r)$ to the pair potential $v(r)$ and the pair correlation function $h(r) = g(r) - 1$, according to

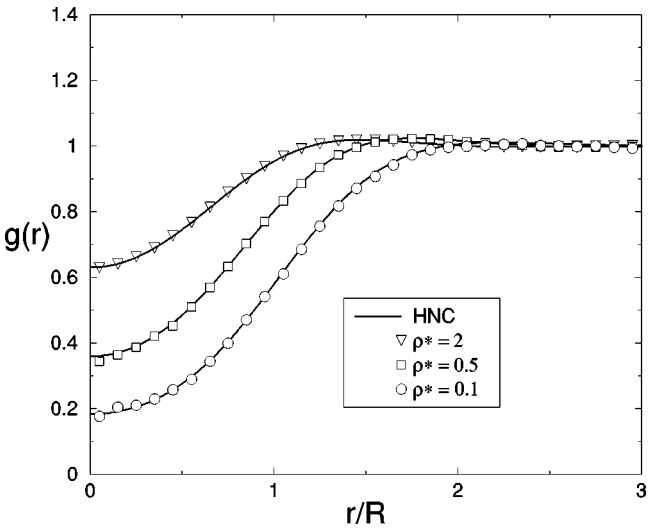

FIG. 2. Comparison of MC simulations and solutions of the HNC integral equation in a regime relevant for polymer solutions [8] $\beta v(r) = 2\exp[-(r/R)^2]$. The lines are HNC calculations, and the symbols represent MC simulations for different reduced densities ρ^*.

$$c(r) = -\beta v(r) + h(r) - \ln[1 + h(r)], \tag{5}$$

where $\beta = 1/k_B T$. This closure must be combined with the Ornstein Zernike (OZ) relation between $c(r)$ and $h(r)$ [13] to yield a nonlinear integral equation, which must be solved numerically. Examples for $\epsilon^* = 2$ at three reduced densities ρ^* are shown in Fig. 2, and compared to the results of MC simulations.

The key feature is that the ''soft'' correlation hole is gradually reduced as ρ^* increases, a behavior typical of finite core potentials, which leads to overlap and ideal-gas-like behavior of $g(r)$ in the high density limit. Note that the HNC results are indistinguishable from the MC data, so that for $\epsilon^* \simeq 2$ the HNC correlation function will henceforth be considered as providing an ''exact'' reference to gauge simpler theories. The simplest is the RPA [13,14], which may be formally derived from the HNC closure (5) by linearizing the logarithm, leading to

$$c(r) = -\beta v(r). \tag{6}$$

Since Fig. 2 clearly shows that the amplitude of $h(r)$ is rather small at high densities, we may expect the RPA closure to become more accurate as the density increases. For the GCM, Eq. (6) and Eq. (2) imply the following FT of $c(r)$

$$\hat{c}(k) = -\epsilon^* \pi^{3/2} R^3 \exp\left[\frac{-k^2 R^2}{4}\right] \tag{7}$$

and the OZ relation immediately yields the following RPA structure factor:

$$S(k) = 1 + \rho \hat{h}(k) = \frac{1}{1 - \rho \hat{c}(k)} = \frac{1}{1 + \alpha \exp[-k^2 R^2/4]}, \tag{8}$$

where we have introduced the dimensionless coupling parameter

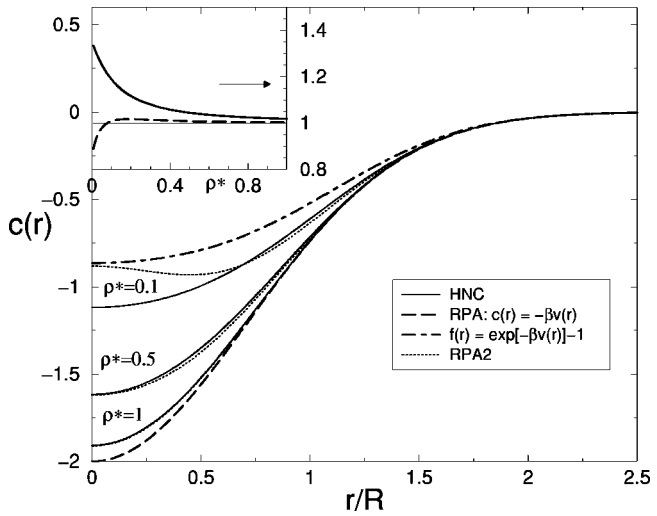

FIG. 3. HNC, RPA, and RPA2 forms of the direct correlation function $c(r)$ for $\beta v(r)=2\exp[-(r/R)^2]$. From top to bottom the densities are $\rho^*=0.1,0.5$, and 1, respectively. Note that the HNC $c(r)$ is bounded by $c_{\mathrm{RPA}}(r)=-\beta v(r)$ from below and $f(r)=\exp[-\beta v(r)]-1$ from above. Inset: Ratio's $\hat{c}_{\mathrm{RPA}}(0)/\hat{c}_{\mathrm{HNC}}(0)$ (solid line) and $\hat{c}_{\mathrm{RPA2}}(0)/\hat{c}_{\mathrm{HNC}}(0)$ (long-dashed line) vs density ρ^*. For $\rho^*>0.05$, $\hat{c}_{\mathrm{RPA2}}(0)$ is always within 2% of $\hat{c}_{\mathrm{HNC}}(0)$

$$\alpha=\pi^{3/2}\beta\epsilon\rho R^3=\pi^{3/2}\rho^*\epsilon^*. \tag{9}$$

HNC results for $c(r)$ and $S(k)$ at several densities are compared to the RPA predictions in Figs. 3 and 4.

Since $h(r)\geqslant\ln[1+h(r)]$, the HNC direct correlation functions are bounded below by the RPA form (6). Figure 3 also shows that the HNC $c(r)$ appears to be bounded above by the low density approximation

$$c(r)=f(r)=\exp[-\beta v(r)]-1 \tag{10}$$

which corresponds to the lowest order term in the expansion of $c(r)$ in powers of ρ [13]; $f(r)$ is the usual Mayer f function. Figures 3 and 4 also illustrate the point that the simple

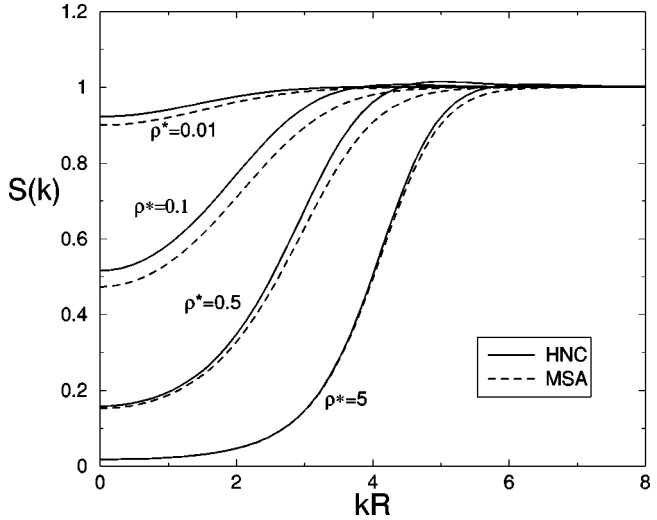

FIG. 4. RPA and HNC forms of the structure factor $S(k)$ for $\beta v(r)=2\exp[-(r/R)^2]$. From top to bottom the densities are $\rho^*=0.01,0.1,0.5,5$, respectively.

RPA becomes very accurate at high densities, so that it is worthwhile to inquire about a correction to Eq. (6). Expanding the logarithm on the right-hand side (RHS) of Eq. (5) to second order in h, one arrives at the following expression for $c(r)$:

$$c(r)=-\beta v(r)+\frac{1}{2}h(r)^2. \tag{11}$$

Solution of the closure (11) and the corresponding OZ relation requires an iterative procedure, as for the full HNC closure. Further simplification amounts to replacing $h(r)$ in Eq. (11) by its RPA form derived from Eq. (8) by FT; we refer to this noniterative approximation as RPA2 [15]:

$$c(r)=-\beta v(r)+\frac{1}{2}h_{\mathrm{RPA}}(r)^2. \tag{12}$$

From Fig. 3 it is clear that $c_{\mathrm{RPA2}}(r)$ is indistinguishable from the HNC results except at low densities ($\rho^*\lesssim 0.2$). The limitations of RPA theory at low densities become apparent by considering the resulting behavior of $g(r)$ at short distance.

The zero separation value is easily derived from the $r\rightarrow 0$ limit of the FT of Eq. (8), with the result

$$g_{\mathrm{RPA}}(0)=1+\frac{\epsilon^*}{\alpha}\mathrm{Li}_{3/2}(-\alpha), \tag{13}$$

where the nth polylogarithm is defined by:

$$\mathrm{Li}_n(x)=\sum_{k=1}^{\infty}\frac{x^k}{k^n} \tag{14}$$

for $|x|\leqslant 1$. If $\epsilon^*<1$, $g_{\mathrm{RPA}}(0)$ is positive for all densities ρ^*. However, when $\epsilon^*>1$ there is always a reduced density ρ_0^* *below* which $g_{\mathrm{RPA}}(0)<0$, which is unphysical. For example, if $\epsilon^*=2$, $g_{\mathrm{RPA}}(0)<0$, for $\rho^*<\rho_0^*=0.3617$. However, even for $\rho^*<\rho_0^*$, the structure factor $S(k)$ is still reasonably well described by the RPA because the deficiencies of $g(r)$ at small r do not strongly affect $S(k)$. This is also illustrated in the inset of Fig. 3, where $\hat{c}_{\mathrm{RPA2}}(0)$ is seen to approximate the quasiexact HNC result to within 2% for densities $\rho^*\gtrsim 0.05$, which is a significantly lower bound than $\rho_0^*=0.3671$.

C. Thermodynamics of the GCM fluid

Turning now to thermodynamic properties, the equation of state can be calculated via either of two routes [13]: from the compressibility equation

$$\beta P=\int_0^{\rho}\frac{\partial\beta P(\rho')}{\partial\rho'}d\rho'=\int_0^{\rho}[1-\rho'\hat{c}(k=0;\rho')]d\rho', \tag{15}$$

where P denotes the pressure. For soft-core potential systems the virial equation leads to

$$\beta P=\rho+\frac{1}{2}\rho^2\hat{v}(k=0)-\frac{2\pi}{3}\rho^2\int_0^{\infty}r^3\frac{\partial\beta v(r)}{\partial r}h(r)dr. \tag{16}$$

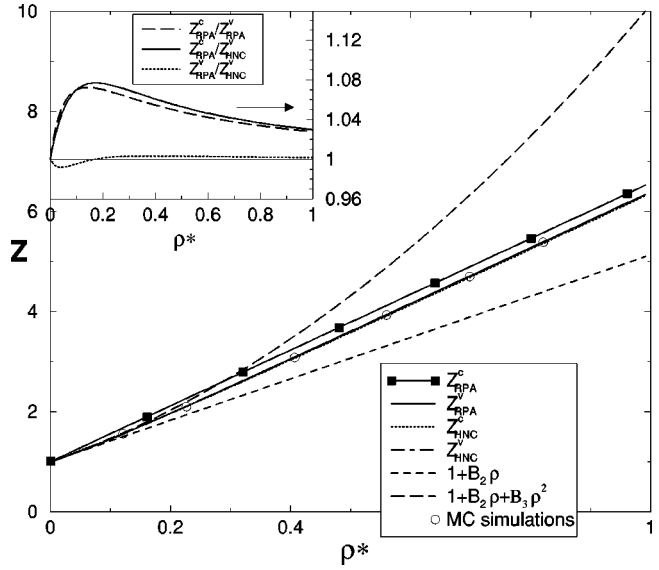

FIG. 5. Compressibility factors ($Z=\beta P/\rho$) from RPA and HNC for a Gaussian potential with $\epsilon^*=2$, compared to MC simulations and to two and three term virial expansions. $Z^v_{\rm RPA}$, $Z^c_{\rm HNC}$, and $Z^v_{\rm HNC}$, are indistinguishable on this scale. Inset: The analytic ratio $Z^c_{\rm RPA}/Z^v_{\rm RPA}=[1-\epsilon^*\aleph(\alpha)/(1+\alpha/2)]^{-1}$ gives a good approximation to $Z^c_{\rm RPA}/Z^v_{\rm HNC}$ and goes to zero as $\rho\to\infty$. The ratio $Z^v_{\rm RPA}/Z^v_{\rm HNC}$ demonstrates that $Z^v_{\rm RPA}$ approximates the true EOS to better than 1% accuracy over the entire density range for $\epsilon^*=2$.

If the correlation functions $h(r)$ and $c(r)$ were known exactly, the two routes would lead to identical equations of state. Approximate theories are not, in general, thermodynamically consistent. However, as shown in Figs. 5–7, the HNC closure yields practically identical values of the pressure over the whole range of densities, even for a repulsion

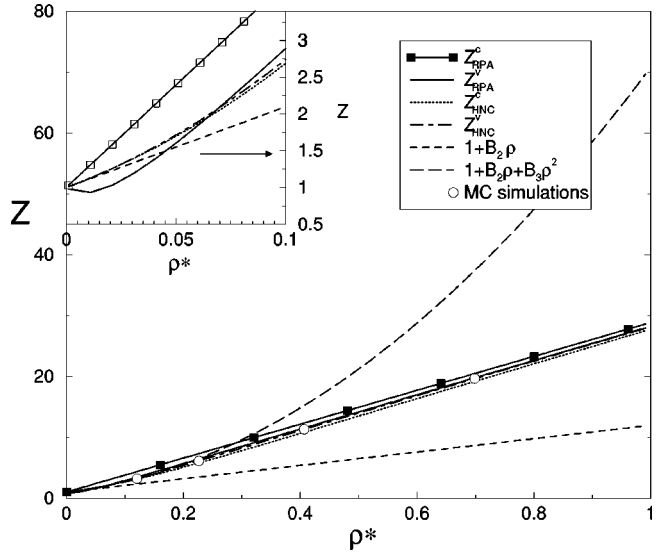

FIG. 6. Compressibility factors from RPA and HNC for a Gaussian potential with $\epsilon^*=10$, compared to MC simulations and to two and three term virial expansions. $Z^v_{\rm RPA}$, $Z^c_{\rm HNC}$, and $Z^v_{\rm HNC}$ are very close over much of the density range. Inset: Compressibility factors at low density, symbols are the same as in the main figure. Note that $Z^v_{\rm RPA}$ shows unphysical behavior for very small ρ^*, which can be understood from the effective virial expansion discussed in Appendix B.

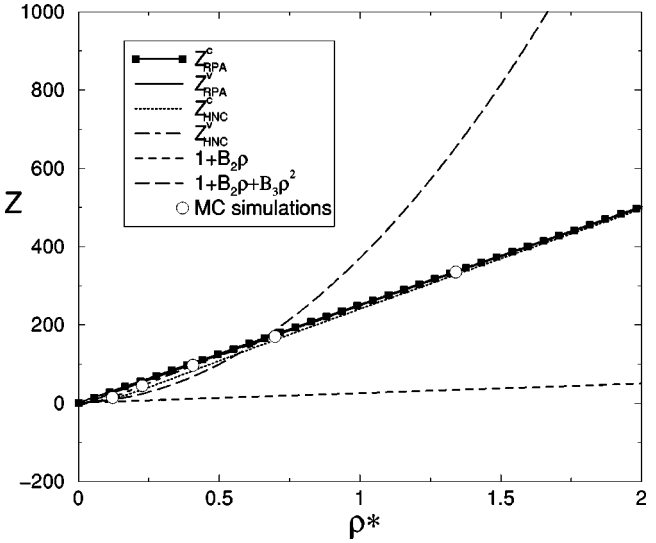

FIG. 7. Compressibility factors from RPA and HNC for a Gaussian potential with $\epsilon^*=90$, compared to MC simulations and to two and three term virial expansions. Again, the HNC virial approximation is nearly exact across the whole density range, and the EOS is that of a mean-field fluid at all but the lowest densities. The low-density limit is further discussed in Appendix B and illustrated in Fig. 15.

as high as $\epsilon^*=90$ (remember that for $\epsilon^*\gtrsim 100$ reentrant crystallization sets in [9,10]). Moreover, the two HNC estimates of the pressure agree closely with the results of MC simulations. These results confirm the conjecture that HNC and RPA become exact for the GCM in the high density limit, but also show that HNC works well for low densities in the fluid regime we consider ($\epsilon^*<100$).

Turning now to the much simpler RPA, it is easily verified from Eqs. (6) and (15) that the dimensionless equation of state (EOS), $Z=\beta P/\rho$, reduces, within the compressibility route, to the simple expression

$$Z^c_{\rm RPA}=1+\frac{1}{2}\rho\beta\hat{v}(k=0) \tag{17}$$

which for the GCM leads to

$$Z^c_{\rm RPA}=1+\frac{1}{2}\alpha. \tag{18}$$

This in turn leads to an excess free energy per particle

$$\frac{\beta F^{\rm ex}}{N}=\frac{1}{2}\rho\beta\hat{v}(k=0)=\frac{1}{2}\alpha \tag{19}$$

identical to that obtained from a van der Waals-like mean-field (MF) theory, so that $Z^c_{\rm RPA}=Z_{\rm MF}$; it also implies that the excess chemical potential is linear in density.

Remembering that the quasiexact HNC direct correlation function is bounded below by the RPA form (6), it is immediately clear from the compressibility equation (15) that one may expect

$$Z<Z^c_{\rm RPA}=Z_{\rm MF}. \tag{20}$$

This conjecture is supported by Eq. (16), which shows that the exact equation of state is given by

$$Z = Z^c_{\mathrm{RPA}} - \frac{2\pi}{3}\rho^2 \int_0^\infty r^3 \frac{\partial \beta v(r)}{\partial r} h(r) dr, \tag{21}$$

which, for the Gaussian core model reduces to

$$Z = 1 + \frac{1}{2}\alpha + \frac{4\alpha}{3\sqrt{\pi}} \int_0^\infty x^4 e^{-x^2} h(x) dx, \tag{22}$$

where the dimensionless spacing $x = r/R$ was introduced. The conjecture (20) is thus true, provided the integral on the RHS of Eq. (22) is negative. This is very likely for sufficiently high temperatures since the HNC results plotted in Fig. 2 show that $h(x)$ is mostly negative.

The integral in Eq. (22) can be calculated analytically within the RPA, leading to the following result for the RPA virial equation of state:

$$Z^v_{\mathrm{RPA}} = 1 + \frac{1}{2}\alpha - \epsilon^* \aleph(\alpha), \tag{23}$$

where

$$\aleph(\alpha) = \frac{1}{2\alpha}[\mathrm{Li}_{3/2}(-\alpha) - \mathrm{Li}_{5/2}(-\alpha)]. \tag{24}$$

$\aleph(\alpha)$ is zero for $\alpha = 0$, has a maximum of 0.0908 at $\alpha = 7.8$, and goes to zero for $\alpha \to \infty$, which implies that for any ϵ^*, the RPA becomes thermodynamically consistent in the high density limit.

Interestingly, within the RPA2, the compressibility EOS may also be solved analytically and yields exactly the same result (23) as the virial EOS in the RPA (i.e., $Z^c_{\mathrm{RPA2}} = Z^v_{\mathrm{RPA}}$), suggesting that the latter is more accurate than the MF or RPA compressibility equation of state (17). In fact, as shown in Figs. 5–7, the RPA virial equation of state is virtually indistinguishable from the practically self-consistent HNC results and the MC simulations, except at very low reduced densities ρ^*. Figure 7 demonstrates that the mean-field approximation (17) is still surprisingly good, even for an interaction as large as $\epsilon^* = 90$, just below the value where freezing sets in. This implies that the hard-sphere limit, envisioned by Stillinger [9], is still not reached at such a strong interaction, and that the Gaussian core model behaves as a ''mean-field fluid'' (MFF) over a wide temperature and density range.

Perhaps the most striking result is the persistence of the linear slope of the equation of state to such low densities [16]. The slope differs, however, from that determined by the (smaller) second virial coefficient. This is further discussed in Appendix B, where it is shown that the standard virial expansion of the equation of state [13] has a very small radius of convergence for the GCM, and is of limited use for this model, contrarily to the case of the hard sphere fluid [17].

III. THE GCM NEAR A WALL

In view of the success of the HNC and RPA theories for the GCM in the homogeneous bulk fluid phase, it is of interest to ascertain the validity of these approximations under inhomogeneous conditions, e.g., in the presence of an external potential $\phi(\mathbf{r})$ acting on the particles. In this section we shall consider more specifically the density profiles of GCM particles near a hard wall, using the formalism of density functional theory (DFT). In an external potential the density of particles will change from a constant bulk value ρ_b to a spatially varying local density $\rho(\mathbf{r})$. The grand potential of the inhomogeneous fluid in equilibrium with a bulk reservoir fixing the chemical potential μ, may be cast in the generic form [18]

$$\beta\Omega_v[\rho(\mathbf{r})] = \beta\mathcal{F}^{\mathrm{in}}[\rho(\mathbf{r})] - \int d\mathbf{r}[\beta\mu - \beta\phi(r)]\rho(\mathbf{r}), \tag{25}$$

where the intrinsic free energy functional $\mathcal{F}^{\mathrm{in}}$ naturally splits into ideal and excess parts, $\mathcal{F}^{\mathrm{id}}$ and $\mathcal{F}^{\mathrm{ex}}$. The latter is an unknown functional of the local density $\rho(\mathbf{r})$. When the inhomogeneity is not too strong, the excess part $\mathcal{F}^{\mathrm{ex}}$ may be expanded in a functional Taylor series in the deviation of the local density $\rho(\mathbf{r})$ from the bulk density ρ_b. If the expansion is truncated after second order the HNC functional results

$$\begin{aligned}\beta\Omega_v[\rho(\mathbf{r})] = \beta\Omega[\rho_b] &+ \int d\mathbf{r}'\beta\phi(\mathbf{r}')\rho(\mathbf{r}') \\ &+ \int d\mathbf{r}'\{\rho(\mathbf{r}')\ln[\rho(\mathbf{r}')/\rho_b] - \rho(\mathbf{r}') + \rho_b\} \\ &- \frac{1}{2}\int d\mathbf{r}d\mathbf{r}'[\rho(\mathbf{r}) - \rho_b]c_b^{(2)}(|\mathbf{r}-\mathbf{r}'|)[\rho(\mathbf{r}') \\ &- \rho_b].\end{aligned} \tag{26}$$

This functional is to be minimized with respect to $\rho(\mathbf{r})$, and the resulting Euler-Lagrange equation reads

$$\rho(\mathbf{r}) = \rho_b \exp\left[-\beta\phi(\mathbf{r}) + \rho_b \int d\mathbf{r}' c_b^{(2)}(|\mathbf{r}'-\mathbf{r}|)\left(\frac{\rho(\mathbf{r}')}{\rho_b} - 1\right)\right] \tag{27}$$

which is the familiar HNC approximation for the density profile $\rho(\mathbf{r})$ in terms of the external potential and the *bulk* direct correlation function $c_b^{(2)}(r) \equiv c(r)$. Given $c(r)$ from the previous HNC calculations of the pair structure in the bulk, Eq. (27) may be solved iteratively for any $\phi(\mathbf{r})$. If $c(r)$ is replaced by its RPA form (6), then Eq. (27) reduces to the MF form

$$\rho(\mathbf{r}) = \rho_b \exp\left[-\beta\phi(\mathbf{r}) - \rho_b \int d\mathbf{r}' \beta v(|\mathbf{r}-\mathbf{r}'|)\left(\frac{\rho(\mathbf{r}')}{\rho_b} - 1\right)\right]. \tag{28}$$

Equation (28) also follows directly from the standard mean field approximation (MF-DFT) for for the intrinsic free energy functional [18]

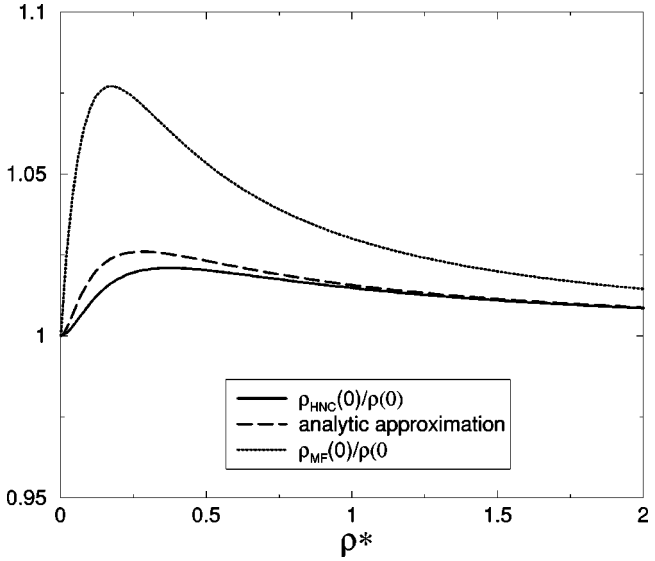

FIG. 8. Ratio $\rho_{\mathrm{HNC}}(0)/\rho(0)$ from Eq. (31) compared to the analytic ratio obtained from the RPA2 approximation to Eq. (31) for $\epsilon^*=2$. Also included is the ratio $\rho_{\mathrm{MF}}(0)/\rho(0)\simeq Z^c_{\mathrm{RPA}}/Z^v_{\mathrm{HNC}}$. Clearly the HNC is the better approximation, even though it does not satisfy the sum rule of Eq. (30).

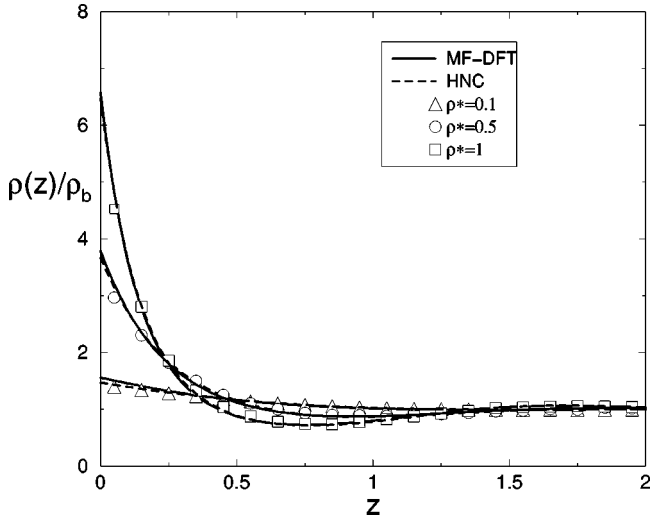

FIG. 9. Density profiles from HNC and the MF-DFT for Gaussian particles ($\epsilon=2, R=1$) near a hard wall. Symbols are for MC simulations at three densities, the solid lines are from the MF-DFT approach, and the dashed lines are from the HNC approach. The two theories and simulation agree to within the accuracy of the graph for $\rho^*=0.5$ and $\rho^*=1$, but small discrepancies appear for $\rho^*=0.1$, where the HNC is slightly more accurate.

$$\beta\mathcal{F}^{\mathrm{in}}[\rho(\mathbf{r})]=\beta\mathcal{F}^{\mathrm{id}}+\frac{1}{2}\int d\mathbf{r}d\mathbf{r}'\,\beta v(\mathbf{r},\mathbf{r}')\rho(\mathbf{r})\rho(\mathbf{r}'), \tag{29}$$

which, in a different context, is identical to the functional used to derive the Poisson-Boltzmann theory for ionic fluids if $v(\mathbf{r},\mathbf{r}')$ is taken to be the Coulomb potential and ρ the charge density.

Specializing to the case of a planar wall coinciding with the x-y plane, and confining the particles to the $z\geqslant 0$ half-space, without any additional external potential, we note that the density profile $\rho(z)$ satisfies the contact condition [19]

$$\rho(z=0)=\beta P, \tag{30}$$

where P is the pressure exerted by the particles on the wall, equal to the bulk pressure in the absence of an external potential. The sum rule (30) is satisfied by the MF-DFT approach, where $\rho_{\mathrm{MF}}(0)=\beta P_{\mathrm{MF}}=\rho_b Z_{\mathrm{MF}}$, with Z_{MF} defined by Eq. (17) since $Z_{\mathrm{MF}}=Z^c_{\mathrm{RPA}}$. However, the sum rule is not satisfied by the (more accurate) HNC approximation (27), which instead leads to [20]

$$\rho(0)=\frac{1}{2}\rho_b\left[1+\left(\frac{\partial\beta P}{\partial\rho_b}\right)_T\right]. \tag{31}$$

This reduces to the exact result (30) provided the pressure is a quadratic function of the bulk density. This is very nearly true over a wide range of densities, as shown in the previous section. In particular the simple RPA compressibility (or MF) EOS (18), which provides a fair representation of the numerical HNC results, is of the necessary linear form to make Eq. (30) and Eq. (31) compatible. The deviations from the sum rule (30) may be traced back to the slight nonlinearity of Z_{HNC}, as demonstrated in the inset of Fig. 5 and in Fig. 8. The relative error does not exceed 3% for $\epsilon^*=2$, although it tends to increase with increasing ϵ^*. In fact, the ratio $\rho_{\mathrm{HNC}}(0)/\rho(0)$ may be estimated from the very accurate RPA2; since $Z^c_{\mathrm{RPA2}}=Z^v_{\mathrm{RPA}}$, the required pressure may be calculated from Eq. (23), while the RPA2 inverse compressibility is calculated to be

$$\left(\frac{\partial\beta P}{\partial\rho}\right)_T=1+\alpha-\frac{\epsilon^*}{2\alpha}[\mathrm{Li}_{1/2}(-\alpha)-\mathrm{Li}_{3/2}(-\alpha)]. \tag{32}$$

The resulting analytic estimate of $\rho_{\mathrm{HNC}}(0)/\rho(0)$ is also shown in Fig. 8; as expected, it gives a good approximation of $\rho_{\mathrm{HNC}}(0)/\rho(0)$. Even though the MF approach exactly satisfies the sum rule (30), the HNC approach, which does not satisfy Eq. (30), is a better approximation. We note that the arguments above can be extended to the popular Percus-Yevick approximation [13], where $\rho_{\mathrm{PY}}(0)/\rho(0)\approx(1+\alpha)^{1/2}/(1+1/2\alpha)$ [20], which, in contrast to the HNC or MF approaches, becomes increasingly less accurate as the density increases.

We have numerically solved the HNC and MF Euler-Lagrange equations (27) and (28) to calculate the density profiles $\rho(z)$ of a GCM near a hard wall, for several values of the bulk density ρ_b. The theoretical profiles are compared in Fig. 9 to the results of MC simulations. The agreement is seen to be excellent, particularly at the higher densities. In fact, within the accuracy of the figure the difference between the HNC and MF approaches is visible only for small z at $\rho=0.1$, where, as expected, the HNC approach is slightly more accurate.

In Fig. 10 we show density profiles for particles interacting with an external potential $\beta\phi(z)=\exp[-z]/z$, a situation similar to that encountered for polymer coils near a wall [8]. Once again, we observe that the HNC and MF-DFT approaches are very close, suggesting that both are very accurate and could potentially be fruitfully combined with the

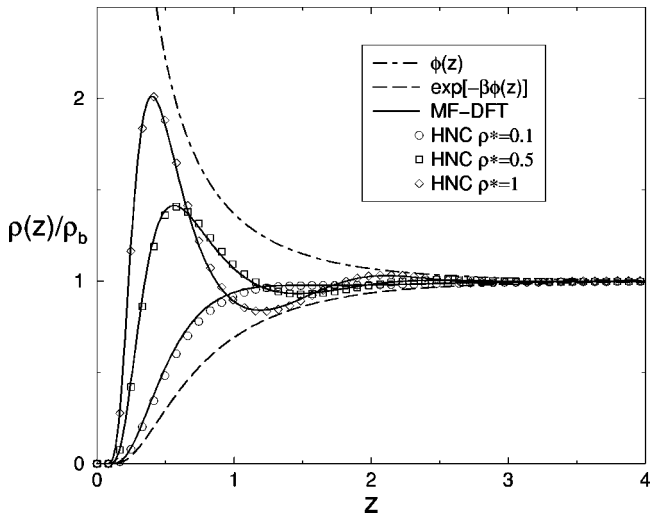

FIG. 10. Density profiles from HNC (symbols) and MF-DFT (lines) for Gaussian particles ($\epsilon^*=2, R=1$) interacting with an external potential $\beta\phi(z)=\exp[-z]/z$.

effective potentials between polymer center of mass [8] to derive a full DFT for polymer solutions in complex geometries. In summary then, the results of this section confirm that the model considered indeed behaves as a ''mean-field fluid'' under inhomogeneous conditions.

IV. PHASE SEPARATION IN TWO-COMPONENT REPULSIVE GAUSSIAN MIXTURES

Since the underlying polymer mixtures exhibit interesting phase behavior under a variety of physical conditions, it is natural to consider binary mixtures of Gaussian core mixtures, interacting via pair potentials

$$\beta v_{\nu\mu}(r)=\epsilon^*_{\nu\mu}\exp[-(r/R_{\nu\mu})^2], \tag{33}$$

where the species indices $1\leqslant\nu,\mu\leqslant 2$. The total number density is still denoted by $\rho=(N_1+N_2)/V$, while the concentration variable $x=N_2/N$. We are interested in the possibility of a phase separation, or demixing transition, of the two species. The thermodynamic stability conditions for any binary mixture can be expressed in terms of the Helmholtz free energy per particle $f(x,v)=F(N_1,N_2,V)/N$, considered as a function of the intensive variables x and v (or $\rho=1/v$), for any fixed temperature. These conditions are [21]

$$\left(\frac{\partial^2 f}{\partial v^2}\right)_x>0, \tag{34a}$$

$$\left(\frac{\partial^2 f}{\partial x^2}\right)_v>0, \tag{34b}$$

$$\left(\frac{\partial^2 f}{\partial v^2}\right)_x\left(\frac{\partial^2 f}{\partial x^2}\right)_v-\left(\frac{\partial^2 f}{\partial v\,\partial x}\right)^2>0. \tag{34c}$$

The first inequality expresses mechanical stability (i.e., positive compressibility), the second is the condition for stability against spontaneous demixing at constant volume, while the last inequality ensures stability at constant pressure; it is equivalent to the more familiar condition $[\partial^2 g(x,P)/\partial x^2]_P>0$, where g is the Gibbs free energy per particle. We note that if either of the first two stability conditions (34a) or (34b) are violated, the more restrictive stability condition (34c) is violated as well. Spinodal instability occurs when Eq. (34c), is satisfied as an equality. The condition is equivalent to the $k\to 0$ divergence of the concentration-concentration structure factor

$$S_{cc}(k)=x^2S_{11}(k)+(1-x)^2S_{22}(k)-2x(1-x)S_{12}(k), \tag{35}$$

where the $S_{\nu\mu}(k)$ are the usual partial structure factors [13]. From the OZ relations for a binary mixture it is easily inferred that $S_{cc}(0)$ diverges when

$$[1-(1-x)\rho\hat{c}_{11}(0)][1-x\rho\hat{c}_{22}(0)]-x(1-x)\rho^2[\hat{c}_{12}(0)]^2=0. \tag{36}$$

We now examine the implications of these conditions within the MF approximation, which we have shown to yield reliable results, except at low reduced density ρ^*. The MF free energy (19), properly generalized to the binary situation, reads

$$f(x,\rho)=f^{\rm id}(\rho)+f^{\rm mix}(x)+\frac{1}{2}\rho\hat{V}_0(x), \tag{37}$$

where the first, ideal gas, term is irrelevant in the subsequent considerations, $f^{\rm mix}$ is the ideal mixing term

$$f^{\rm mix}(x)=x\ln x+(1-x)\ln(1-x), \tag{38}$$

and the MF interaction term is

$$\hat{V}_0(x)=(1-x)^2\beta\hat{v}_{11}(0)+2x(1-x)\beta\hat{v}_{12}(0)+x^2\beta\hat{v}_{22}(0). \tag{39}$$

The $\{\beta\hat{v}_{\nu\mu}(0)\}$ are the $k\to 0$ limits of the FTs of the interaction potentials. In fact, the MF free energy (37) has the same mathematical form as a second-virial theory which would be valid for very low densities [22].

With the MF free energy (37), the stability conditions (34a)–(34c) reduce to

$$1+\rho\hat{V}_0(x)>0, \tag{40a}$$

$$1-\rho x(1-x)\chi>0, \tag{40b}$$

$$1+\rho\hat{V}_1(x)-\rho^2x(1-x)\Delta>0, \tag{40c}$$

respectively, where the following parameters were defined:

$$\chi=2\beta\hat{v}_{12}(0)-[\beta\hat{v}_{11}(0)+\beta\hat{v}_{22}(0)], \tag{41}$$

$$\Delta=[\beta\hat{v}_{12}(0)]^2-\beta\hat{v}_{11}(0)\beta\hat{v}_{22}(0), \tag{42}$$

$$\hat{V}_1(x)=(1-x)\beta\hat{v}_{11}(0)+x\beta\hat{v}_{22}(0). \tag{43}$$

Equation (40a) can only be violated if the potentials themselves violate a two-component extension of Eq. (A5) from

Appendix A, which is a necessary (but not sufficient) condition for the existence of a well-defined thermodynamic limit. The limit of stability of the mixture (i.e., the spinodal line) at constant volume or pressure is reached when the inequalities (40b) and (40c) turn into equalities; the latter condition also follows from Eq. (36), when the $\hat{c}_{\nu\mu}$ are replaced by their RPA limits $\hat{c}_{\nu\mu}(k) = -\beta\hat{v}_{\nu\mu}(k)$. Demixing at constant volume is possible, provided $\chi > 0$; the density along the spinodal is then easily calculated to be

$$\rho_s(x) = \frac{1}{x(1-x)\chi}. \tag{44}$$

Demixing at constant pressure is only possible provided $\Delta > 0$. The corresponding density along the spinodal satisfies

$$\rho_s(x) = \frac{\hat{V}_1(x) + \sqrt{\hat{V}_1(x)^2 + 4x(1-x)\Delta}}{2x(1-x)\Delta}, \tag{45}$$

the pressure along the spinodal is

$$\beta P_s(x) = \rho_s(x) + \frac{1}{2}\rho_s^2(x)\hat{V}_0(x), \tag{46}$$

and the critical consolute point is determined by the condition

$$\frac{dP_s(x)}{dx} = 0. \tag{47}$$

The simple quadratic expression (46) for the pressure P, is easily inverted to obtain an expression for the spinodal density as a function of concentration x and pressure P.

We now apply these general considerations within the MF framework to the binary Gaussian core model for which

$$\beta\hat{v}_{\nu\mu}(0) = \pi^{3/2}\epsilon^*_{\nu\mu}R^3_{\nu\mu}. \tag{48}$$

Inserting the binary GCM expression for $\hat{v}_{\nu\mu}(0)$ into expressions (42) and (43) for χ and Δ, we find that phase-separation at constant volume or at constant pressure is possible provided

$$\chi = \pi^{3/2}[2\epsilon^*_{12}R^3_{12} - (\epsilon^*_{11}R^3_{11} + \epsilon^*_{22}R^3_{22})] > 0 \tag{49}$$

or

$$\Delta = \pi^3[(\epsilon^*_{12})^2R^6_{12} - \epsilon^*_{11}\epsilon^*_{22}R^3_{11}R^3_{22})] > 0. \tag{50}$$

In order to focus on physically relevant values of the parameters $\epsilon^*_{\nu\mu}$ and $R_{\nu\mu}$, it is important to make contact with known results for polymer coils in a good solvent [6,7]. Simulations on binary solutions of self-avoiding polymer coils carried out in the low concentration limit [7] suggest that the effective pair potentials between centers of mass are reasonably well represented by the Gaussian form (33), with

$$\epsilon^*_{12} \leqslant \epsilon^*_{11} \simeq \epsilon^*_{22} \tag{51}$$

and

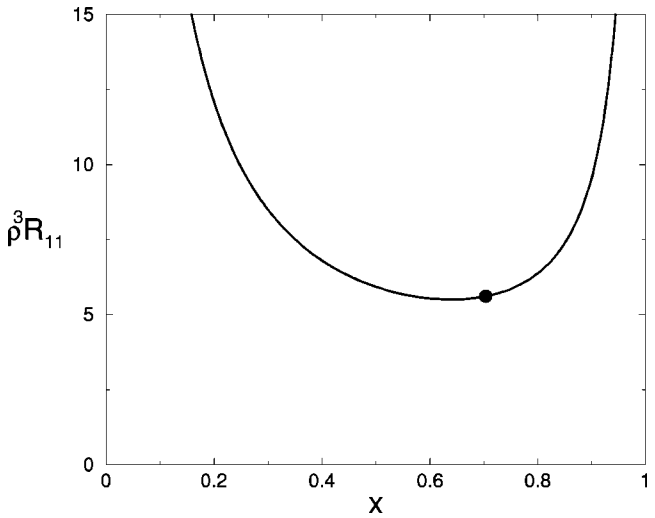

FIG. 11. Constant pressure spinodal (45) for parameters taken from simulations of $L = 100$ and $L = 200$ monomer effective polymer CM potentials [7]. The x axis denotes the composition $x = x_2 = N_2/N$. The y axis denotes the density ρR^3_{11}, where R_{11} is the = radius of gyration R_G for the $L = 200$ polymers. The dot is the critical point at ($x = 0.70$, $\rho R^3_{11} = 5.6$).

$$R^2_{12} \simeq \frac{1}{2}(R^2_{11} + R^2_{22}). \tag{52}$$

The relation (51) between the $\epsilon_{\nu\mu}$ favors mixing. On the other hand $R_{12} > 1/2(R_{11} + R_{22})$, which resembles the positive nonadditivity that can drive demixing in hard-core mixtures [24]. Substituting Eq. (52) into Eq. (49), we find that a spinodal instability of the mixture is possible at constant volume provided

$$\frac{\epsilon^*_{12}}{\epsilon^*_{11}} > \sqrt{2}\frac{1 + (R_{22}/R_{11})^3}{[1 + (R_{22}/R_{11})^2]^{3/2}} \geqslant 1 \tag{53}$$

which contradicts the requirement (51). On the other hand, if Eq. (52) is substituted into Eq. (50), demixing at constant pressure may occur provided

$$\frac{(\epsilon^*_{12})^2}{\epsilon^*_{11}\epsilon^*_{22}} > \left[\frac{2(R_{22}/R_{11})}{1 + (R_{22}/R_{11})^2}\right]^3 \leqslant 1, \tag{54}$$

which is compatible with the requirement (51).

More specifically, we have chosen values of the parameters $\epsilon^*_{\nu\mu}$ and $R_{\nu\mu}$ appropriate for a polymer mixture of self-avoiding polymers of $L = 200$ (species 1) and $L = 100$ (species 2) monomers [7,23]. The resulting spinodal line (45) in the x-ρ plane, calculated from the MF free energy (37) with (48), is shown in Fig. 11. Phase separation into two solutions of different composition x occurs above a critical density $\rho^*_c = 5.6/R^3_{11}$ and critical composition $x_c = 0.70$. Note that since all terms in the free energy are of entropic origin, the temperature scales out, i.e., the mixture behaves as an athermal system. In view of the remarkable accuracy of the MF theory at high density, as illustrated in Sec. II and III for the one component GCM fluid, we expect the phase diagrams, calculated within MF (or equivalently RPA) to be reliable;

full calculations of the binodal line, based on RPA2 and HNC theories, will be reported elsewhere.

V. CONCLUSIONS

The calculations carried out in this paper, and in related work [8], lead to the conclusion that a system of classical particles interacting via a repulsive Gaussian core potential behaves as a weakly correlated ''mean field fluid'' over a wide range of temperatures and densities. In fact for any temperature there is always a (surprisingly low) density beyond which the excess free energy per particle is a linear function of density and the resulting excess pressure increases as a quadratic function of the density. On the other hand, in the opposite low density regime, a virial expansion of the equation of state in powers of the density appears to converge only at extremely low densities. This is in sharp contrast to hard-core systems, for which the virial expansion provides a good estimate of the equation of state up to relatively high packing fractions [17], while the pressure diverges near close packing according to a simple free volume picture. At very strong interaction strength ($\epsilon^* \gtrsim 100$), the GCM behaves effectively as a hard core fluid that freezes at intermediate densities, but remelts under further compression to return to mean-field-like behavior [9,10]. The small correlational effects at low and intermediate interaction strengths are adequately described by the simple, analytic RPA2 extension of RPA theory, or by the HNC integral equation (requiring numerical solution), which is nearly thermodynamically consistent over a broad range of temperatures and densities.

The MF theory performs equally well in the inhomogeneous situation of Gaussian core particles near a hard wall. The binary version of the model phase separates at high densities, when the widths of the Gaussian repulsion satisfy the composition rule (52), provided condition (54) is satisfied. This provides an interesting example of phase separation in systems with purely repulsive interactions.

To conclude it seems worthwhile to consider the relevance of the GCM for the description of polymer solutions. The latter enter the semidilute regime when polymer coils start to overlap, i.e., when $\rho^* \sim 3/(4\pi)$. For densities of this order we have seen that the GCM behaves as a ''mean-field fluid,'' with a quadratic density dependence of the pressure. The exponent 2 is close to the 9/4 power observed for the osmotic pressure of semidilute polymer solutions [25]. The difference between the exponent 9/4 and 2 is due in part to the weak, but significant density dependence of the effective pair potential between the centers of mass of self-avoiding polymers [8], which leads to an additional density dependence of the RPA or MF equation of state (17). This possibility is being explored in more detail [26].

The effective polymer-wall potentials derived in Ref. [8] show a significant variation with density. Nevertheless, the form of the $\rho(z)/\rho_b$ for the GCM in a *fixed* external potential follows the same qualitative trends as the distribution of the polymer CM's near a wall, $\rho_{\mathrm{CM}}(z)/\rho_b$, suggesting that the physics of polymer coils near a wall is well captured by the GCM.

The demixing transition of binary Gaussian core mixtures is reminiscent of the tendency of polymers of different molecular weight to phase separate at high concentration and in the melt. Again, further analysis is required to decide if the analogy between the demixing of Gaussian core mixtures and of polymer blends is fortuitous, or has some deeper foundation.

ACKNOWLEDGMENTS

A.A.L. acknowledges support from the Isaac Newton Trust, Cambridge. P.B. acknowledges support from the EPSRC under Grant No. GR/M88839. We thank Christos Likos for helpful correspondence, Bob Evans for suggesting the mean-field DFT approach to us, and David Rowan for a critical reading of the manuscript.

APPENDIX A: THERMODYNAMIC STABILITY OF SOFT-CORE POTENTIAL SYSTEMS

It was pointed out in Sec. II A that the GCM satisfies Ruelle's condition (3) for the existence of a finite thermodynamic limit. In this appendix we give two examples of pair potentials involving a repulsive core and a small *attractive* component which do not satisfy Ruelle's stability condition, and hence belong to the class of potentials referred to by him as ''catastrophic.'' The following considerations are not completely academic, since it has been shown in Ref. [26] that the effective pair potential between the centers of mass of two polymer coils in a good solvent indeed exhibits a small attractive part at distances of the order of several times the radius of gyration R_g for intermediate densities. When the polymer coils are no longer in a good solvent the potentials can develop even larger attractive parts [7].

According to proposition 3.2.2 in Ref. [12], given an interaction energy $V_N^{(2)}$ built up by pair potentials v_2, the grand partition function is finite only if the following two equivalent properties hold for all $N \geqslant 0$ and all $\{\mathbf{r_i}\} \in \mathbf{R^N}$:

$$\sum_i^N \sum_j^N v_2(|\mathbf{r_i} - \mathbf{r_j}|) \geqslant 0 \tag{A1}$$

and

$$V_N^{(2)}(\mathbf{r_1}, \ldots, \mathbf{r_N}) = \sum_{1 \leqslant i < j \leqslant N} v_2(|\mathbf{r_i} - \mathbf{r_j}|) \geqslant -NB \tag{A2}$$

for a $B \geqslant 0$. Note that in Eq. (A1) the double sum includes the self-interaction ($i = j$).

We consider two examples of potentials which do not satisfy these conditions

$$v_A(r) = 1.87 \cos\left[\sqrt{(2+\delta)}\left(\frac{r}{1.7R_G}\right)\right] \exp\left[-\left(\frac{r}{1.7R_G}\right)^2\right], \tag{A3}$$

$$v_B(r) = 1.87 \cos\left[\sqrt{\pi}\left(\frac{r}{1.7R_G}\right)\right] \exp\left[-\left(\frac{r}{1.7R_G}\right)^4\right], \tag{A4}$$

and compare them in Fig. 12 to the polymer CM potential between two isolated $L = 500$ SAW polymer coils. Here δ is an arbitrary positive constant taken to be $\delta = 0.001$ in Fig. 12. Although at first sight they do not appear very different from the purely repulsive polymer potential, they are both ''catastrophic.''

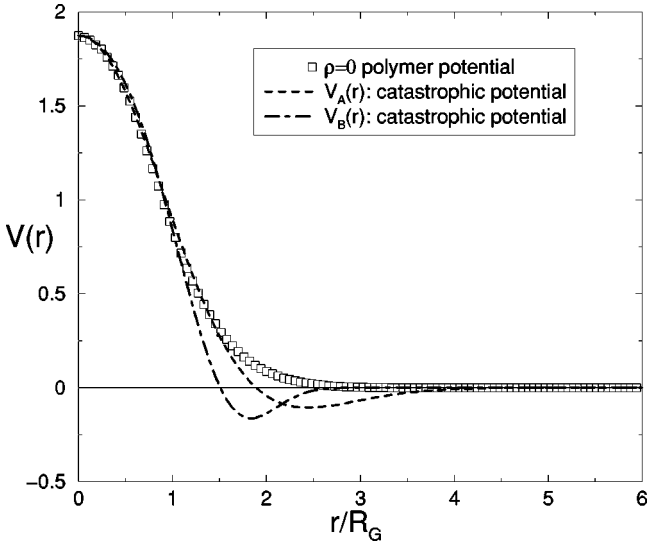

FIG. 12. Two ''catastrophic'' potentials compared to a typical CM potential for two polymers in a good solvent. Potential $v_A(r)$ (A3) violates the conditions (A1) and (A2) for homogeneous fluid configurations, while potential $v_B(r)$ (A4) violates Eqs. (A1) and (A2) only for inhomogeneous configurations like the fcc crystal.

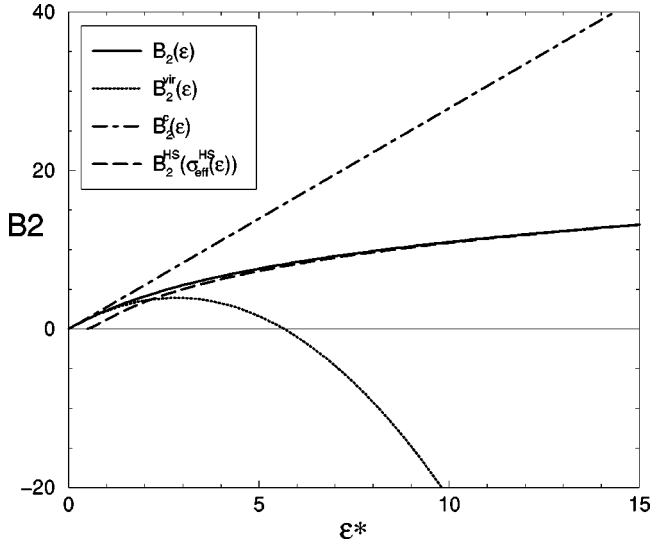

FIG. 13. Second virial coefficients for a Gaussian potential as a function of interaction strength ϵ^* ($B_2^c > B_2 > B_2^{\rm vir}$). Also included is the empirical relation $B_2^{\rm HS}[\sqrt{\ln(2\epsilon^*)}]$, where $B_2^{\rm HS}(\sigma)$ is the hard-sphere second-virial coefficient.

If $\delta > 0$, the first potential, $v_A(r)$, violates a weaker condition than Eq. (A1) or Eq. (A2), namely,

$$\hat{v}(0) = \int v(r) d\mathbf{r} > 0, \tag{A5}$$

which is necessary (but not sufficient) for a thermodynamic limit. When it does not hold, conditions (A1) and (A2) can be violated for a homogeneous ''gas'' with $g(r)=1$. This has a further implication for fluids described by a mean-field free-energy (19), since the inverse compressibility $\partial\beta P/\partial\rho = 1+\beta\hat{v}(0)\rho$ cannot go through zero without violating the condition (A5), which implies that one-component soft-core fluids described by a mean-field EOS cannot support a spinodal instability.

The second potential $v_B(r)$ has an integral $\hat{v}_B(0) > 0$, but it still violates Eqs. (A1) and (A2) for an *inhomogeneous* configuration. For example, for an fcc lattice with single occupancy $\Sigma_i^N \Sigma_j^N v_B(|\mathbf{r_j} - \mathbf{r_i}|) = -0.13N$. The potential is catastrophic because one can always lower the total energy indefinitely through multiple occupancy of the lattice sites.

The θ point in polymer solutions can be defined as the temperature where the effective second osmotic virial coefficient B_2 passes through 0 [7]. Above the θ point the solvent is said to be ''good,'' while below the θ point the solvent is said to be ''poor.'' Simulations of a model for two polymers in a poor solvent show that the effective pair potential is no longer strictly positive definite below the θ point [7], implying that the pair potentials can become catastrophic. In fact, for the type of polymer CM potentials considered, this seems to occur just below the θ point temperature where $B_2 = 0$. It is tempting to speculate that the coil-globule transition, which also typically occurs slightly below the θ temperature, is related to the point at which the effective pair potential becomes catastrophic. However, it is not yet clear whether the pair-potential picture of polymer solutions [8] remains valid for poor solvents.

APPENDIX B: VIRIAL EXPANSION FOR THE GCM FLUID

In this appendix we briefly consider the convergence of the virial expansion of the equation of state of the GCM in powers of the density ρ. The FT of the Mayer f function in Eq. (10) is given by the convergent sum

$$\hat{f}(k) = \pi^{3/2} \sum_{n=1}^{\infty} \frac{\exp\left(-\frac{k^2}{4n}\right)(-\epsilon^*)^n}{n! n^{3/2}}. \tag{B1}$$

Here the width parameter R in the Gaussian potential (1) has been chosen as unit of length for convenience. The second and third virial coefficients B_2 and B_3 of the GCM can then be expressed as the following convergent sums:

$$B_2 = -\frac{1}{2}\hat{f}(0) = -\frac{\pi^{3/2}}{2} \sum_{n=1}^{\infty} \frac{(-\epsilon^*)^n}{n! n^{3/2}}, \tag{B2}$$

$$B_3 = -\frac{1}{3}\pi^3 \sum_{i=1}^{\infty}\sum_{j=1}^{\infty}\sum_{k=1}^{\infty} \frac{(-\epsilon^*)^{i+j+k}}{i!j!k!(ij+jk+ik)^{3/2}}. \tag{B3}$$

The variations of B_2 and B_3 with ϵ^* are shown in Figs. 13 and 14; both virial coefficients are always positive.

The virial expansion of the equation of state reads

$$Z = \frac{\beta P}{\rho} = 1 + B_2\rho + B_3\rho^2 + \mathcal{O}(\rho^3) \tag{B4}$$

and the results from the two and three term series are compared in Figs. 5–7 of Sec. II to the predictions of the RPA and HNC theories, and to MC simulations for $\epsilon^* = 2, 10$, and 90. The virial expansion is seen to break down very early. In

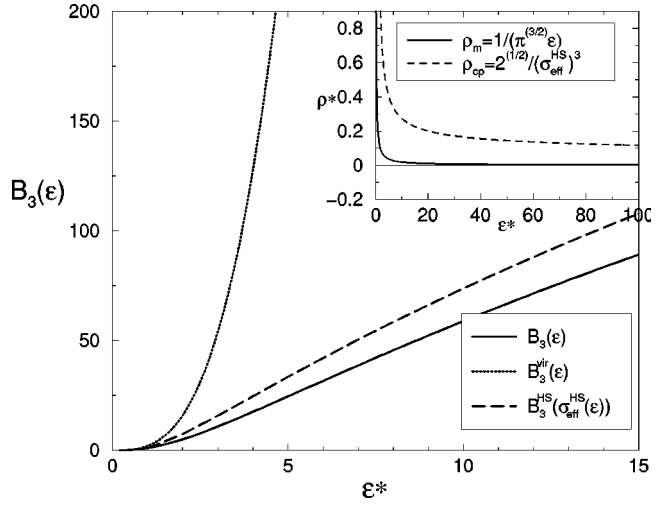

FIG. 14. Third virial coefficients for a Gaussian potential as a function of interaction strength ϵ^*. $B_3^c=0$, $B_3^{\rm vir}>B_3$. Also included is the empirical relation $B_3(\epsilon^*)=B_3^{\rm HS}[\sqrt{\ln(2\epsilon^*)}]$, where $B_3^{\rm HS}(\sigma)$ is the hard-sphere third-virial coefficient. Inset: $\rho_m=1/(\pi^{3/2}\epsilon^*)$ is the maximum density for which the RPA virial EOS (23) can be written as an expansion in powers of the density. $\rho_{\rm cp}=\sqrt{2}/(\sigma_{\rm eff}^{\rm HS})^3$ is the density at which the effective hard-sphere system with the same second virial coefficient as the GCM would be close-packed.

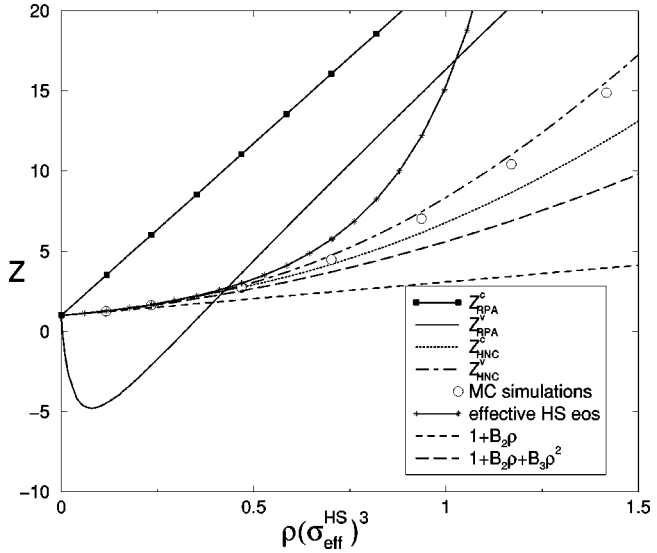

FIG. 15. Z vs $\rho(\sigma_{\rm eff}^{\rm HS})^3$ in the low density limit. Here $\epsilon^*=90$ so that $(\sigma_{\rm eff}^{\rm HS})=2.27$; $\rho(\sigma_{\rm eff}^{\rm HS})^3=1$ corresponds to $\rho^*=0.085$. For low effective density the EOS follows the hard-sphere EOS (here approximated by the Carnahan-Starling form [13]). For higher densities the fluid moves towards the mean-field fluid limit (see Fig. 7). Note that the two RPA expressions for the EOS are very poor approximations in this low density regime.

particular, although the MF EOS, which becomes very accurate at high density, predicts a linear variation of Z with density, the slope differs more and more from B_2 as the interaction strength ϵ^* increases. Adding the B_3 contribution leads to rapid deterioration of the predicted EOS as the density increases.

The shortcoming of the virial expansion in powers of density is further illustrated by considering the RPA. From Eqs. (18) and (23), one may extract the following compressibility and virial estimates of the second and third virial coefficients

$$B_2^c=\frac{1}{2}\pi^{3/2}\epsilon^*, \quad B_3^c=0, \tag{B5}$$

$$B_2^{\rm vir}=\frac{1}{2}\pi^{3/2}\epsilon^*\left(1-\frac{\sqrt{2}}{8}\epsilon^*\right), \quad B_3^{\rm vir}=\frac{\pi^3(\epsilon^*)^3}{9\sqrt{3}}. \tag{B6}$$

As shown in Figs. 13 and 14, the exact virial coefficients are bracketed by the virial and compressibility estimates extracted from the RPA

$$B_2^c>B_2>B_2^{\rm vir}, \tag{B7}$$

$$B_3^{\rm vir}>B_3>B_3^c=0. \tag{B8}$$

The large deviations shown in Figs. 13 and 14 imply that, in contrast to the case at high densities, the RPA is expected to perform poorly at very low densities and large ϵ^*, where it is thermodynamically inconsistent. In fact, $B_2^{\rm vir}$ even goes negative for $\epsilon^*\gtrsim 5.7$. The effect this has on the RPA virial EOS is demonstrated in the inset of Fig. 6 and in Fig. 15. However, even though for $\epsilon^*=2$, $B_2^{\rm vir}$ is 13% less than B_2, and $B_3^{\rm vir}$ is over 300% larger than B_3, $Z_{\rm RPA}^v$ remains within 1% of the exact EOS over the entire density range. Thus, in spite of the fact that the RPA virial approximation grossly misrepresents the first two virial coefficients, it nevertheless accurately describes the EOS, implying that the density is not a good expansion parameter for the GCM fluid phase.

A further hint at the breakdown of the virial expansion comes from summing the virial series to all orders in the high-temperature limit, where, from the diagramattic representation of the virial coefficients [13], it can be shown that the B_n are given by

$$B_n=-\frac{1}{2}\pi^{3(n-1)/2}\frac{(-\epsilon^*)^n(n-1)}{n^{5/2}}+\mathcal{O}(\epsilon^*)^{n+1} \tag{B9}$$

for $n\geqslant 3$. When $B_2^{\rm vir}$ (B6) is added, this recovers exactly the virial RPA equation of state (23), which can only be expanded in powers of density for $\alpha<1$, i.e., for

$$\rho^*<\rho_m^*=\frac{1}{\pi^{3/2}\epsilon^*}\approx 0.1796/\epsilon^*. \tag{B10}$$

This implies that in the high-temperature limit, the virial expansion does not converge for densities higher that ρ_m^*. For $\epsilon^*=2$, there is no convergent density expansion of the RPA virial EOS for $\rho^*>\rho_m^*\approx 0.0898$. A similar breakdown in convergence may be expected for the exact virial expansion. The physical reason for this lack of convergence lies in the possibility of multiple overlap of soft core particles, giving much more weight to higher order cluster integrals compared to the case of fluids with hard-core interactions.

At large enough ϵ^*, the overlap probability becomes exponentially small, and the GCM can be mapped onto an effective hard-sphere system [9,10]. One possible criterion for the mapping is to equate the second virial coefficients. From this we obtain an effective hard-sphere radius of

$$\sigma_{\rm eff}^{\rm HS}(\epsilon) = \left(\frac{3}{2\pi} B_2(\epsilon^*) \right)^{1/3} \tag{B11}$$

which for $\epsilon^* > 1$ is well approximated by the empirical expression $\sigma_{\rm eff}^{\rm HS} \approx \sqrt{\ln(2\epsilon^*)}$. For large ϵ^* and low densities, the equation of state resembles that of hard spheres (see, e.g., Fig. 15), suggesting that a virial expansion does indeed exist for low densities. We note that for this large value of ϵ^*, the true virial expansion appears to have a larger radius of convergence than that of the RPA virial EOS, for which $\rho_m(\sigma_{\rm eff}^{\rm HS})^3 \approx 0.023$. For $\epsilon^* \gtrsim 100$ there is a freezing transition at roughly the density expected for the effective hard-sphere system $[\rho(\sigma_{\rm eff}^{\rm HS})^3 \approx 1]$, not far above which any effective virial expansion is expected to break down (see, e.g., the inset of Fig. 14). In fact, since Gaussian potentials do not have an infinitely hard core, it is possible to achieve much higher densities than are normally available to simple liquids. At the lowest densities the fluid is described by a linear second virial theory EOS, but as the density increases, this rapidly turns over to a mean-field-like linear EOS with a different (larger) slope. Thus, even though the EOS is well described by a first order polynomial in the density ρ it is not at all equivalent to a second virial theory, and the density is generally not a good expansion parameter.

[1] D. Chandler, J.D. Weeks, and H.C. Anderson, Science **220**, 787 (1983).

[2] M. Baus, J. Phys.: Condens. Matter **2**, 2111 (1990).

[3] D. Frenkel, in *Liquids, Freezing, and the Glass Transition*, edited by J.P. Hansen, D. Levesque, and J. Zinn-Justin (North Holland, Amsterdam, 1991).

[4] P.J. Flory and W.R. Krigbaum, J. Chem. Phys. **18**, 1086 (1950).

[5] A.Y. Grosberg, P.G. Khalatur, and A.R. Khokhlov, Makromol. Chem., Rapid Commun. **3**, 709 (1982).

[6] B. Krüger, L. Schäfer, and A. Baumgärtner, J. Phys. (France) **50**, 319 (1989).

[7] J. Dautenhahn and C.K. Hall, Macromolecules **27**, 5399 (1994), and references therein.

[8] A.A. Louis, P.G. Bolhuis, J.P. Hansen, and E.J. Meijer, Phys. Rev. Lett. **85**, 2522 (2000).

[9] F.H. Stillinger, J. Chem. Phys. **65**, 3968 (1976).

[10] A. Lang, C.N. Likos, M. Watzlawek, and H. Löwen, J. Phys.: Condens. Matter **12**, 5087 (2000); e-print cond-mat/0007089.

[11] We note that in the polymer literature the crossover density between the dilute and semi-dilute regime is often denoted by a fixed density $\rho^* \approx 3/(4\pi R_G^3)$. However, in keeping with traditional usage in the theory of simple fluids [13], we prefer to use $\rho^* = \rho R^3$ as a reduced density.

[12] D. Ruelle, *Statistical Mechanics: Rigorous Results* (Benjamin, London, 1969).

[13] J. P. Hansen and I.R. McDonald, *Theory of Simple Liquids*, 2nd ed. (Academic Press, London, 1986).

[14] We prefer to use the term RPA instead of MSA, since the latter usually implies a hard core [13].

[15] Instead of expanding the logarithm, one could replace $h(r)$ with $h_{\rm RPA}(r)$ in the full HNC expression for $c(r)$ (5), which would lead to a noniterative equation similar to the one originally proposed by Abe in the context of Coulomb systems [R. Abe, Prog. Theor. Phys. **22**, 213 (1959)]. However, for some densities $h_{\rm RPA}(r) \leqslant -1$, leading to a divergence of the logarithm. To avoid this problem we expand the logarithm to second order in $h(r)$. Of course one could always expand to even higher orders, i.e., to third order would be RPA3 etc.

[16] Of course at the very lowest densities the EOS is again described by a linear second virial theory, but the slope is smaller than that of the MF theory.

[17] W.G. Hoover and F.H. Ree, J. Chem. Phys. **46**, 4181 (1967).

[18] R. Evans, in *Fundamentals of Inhomogeneous Fluids*, edited by D. Henderson (Marcel Dekker, New York, 1992).

[19] D. Henderson, L. Blum, and J.L. Lebowitz, J. Electroanal. Chem. **102**, 315 (1979).

[20] S.L. Carnie, D.Y.C. Chan, D.J. Mitchell, and B.W. Ninham, J. Chem. Phys. **74**, 1472 (1981).

[21] J. S. Rowlinson and F. Swinton, *Liquids and Liquid Mixtures*, 3rd ed. (Butterworths, London, 1982).

[22] The $v_{\nu\mu}(0)$ would be replaced by the virial coefficients $B_{\mu\nu}$ in Eq. (39); see R. van Roij, Ph.D. thesis, Utrecht, 1996, for a particularly lucid account of the stability of second-virial theories.

[23] Our approach here mirrors that of M. Watzlawek, C.N. Likos, and H. Löwen, Phys. Rev. Lett. **82**, 5289 (1999), where the low-density interaction between star polymers was used to map out the phase behavior of star-polymer solutions at finite densities.

[24] A.A. Louis, R. Finken, and J.P. Hansen, Phys. Rev. E **61**, R1028 (2000).

[25] M. Doi, *Introduction to Polymer Physics* (Oxford University Press, Oxford, 1995).

[26] P. G. Bolhuis, A. A. Louis, J. P. Hansen, and E. J. Meijer, e-print cond-mat/0009093.